Numerical study on laminar flow forced-convection heat transfer for air in a channel with offset plates heated by radiation heat flux

Received February 1997
Revised October 1997
Accepted December 1997

Ahmed Hamza H. Ali, Koki Kishinami, Yutaka Hanaoka, and Jun Suzuki

Department of Mechanical Systems Engineering, Muroran Institute of Technology, Muroran, Japan

Nonemclature

D_h	=	flow hydraulic diameter $2(w \times \mathbf{h})/(w + \mathbf{h})$
g	=	gravitational acceleration
Gr*	=	modified Grashof number eq. (5)
h	=	lower glass cover and back plate spacing
k	=	thermal conductivity
l	=	length of offset plate
L	=	total length of offset plates
n	=	number of elements i, or j
N	=	number of offset plates (L/**l**)
Nu_x	=	local peripheral Nusselt number eq.(23)
$\overline{Nu}$	=	average Nusselt number eq. (24)
p	=	static pressure
P	=	dimensionless pressure eq. (5)
Pr	=	Prandtl number
q	=	heat flux
Re	=	Reynolds number ($u_{in} D_h/\nu$)
T	=	temperature
t	=	offset plate thickness
u, v	=	velocity components in x and y directions respectively
U, V	=	dimensionless velocity components
w	=	offset plates width
x	=	axial horizontal distance measured from inlet edge of the 1st offset plate
y	=	distance in vertical direction

Greek symbols

α	=	absorptance
α*	=	thermal diffusivity
β	=	volume expansion coefficient
ε	=	emittance
θ	=	dimensionless temperature eq. (5)
ρ	=	reflectivity
ρ*	=	density
σ	=	Stefan-Boltzmann constant
τ	=	transmittance
ν	=	kinematic viscosity

Subscripts

abs	=	absorbed radiation
absr	=	offset plates absorber
absr-l	=	lower surface of the offset absorber plates
absr-u	=	upper surface of the offset absorber plates
air	=	flowing air
b	=	bulk temperature
bk	=	back plate
cond	=	conduction
conv	=	convection
e	=	emitted radiation
g, g1 or g2	=	glass, upper or lower covers
i, j	=	element i, or j
in	=	inlet
inc	=	incident
lw	=	long-wave radiation band
out	=	outlet
pl	=	offset plate
rad	=	radiation
sw	=	short-wave radiation band

1. Introduction

Convective heat transfer between a fluid and solid accompanied with radiation mode is a rather complicated phenomenon. It is known that the

International Journal of Numerical Methods for Heat & Fluid Flow
Vol. 8 No. 5, 1998, pp. 539–558.

entrance region of a fluid flow in a duct or between parallel plates is characterized by thin velocity and thermal boundary layers. Hence, the convective heat transfer coefficient therein is substantially larger than at locations farther downstream. To make a promotion of the convective heat transfer coefficient, using offset (interrupted) plates or fin surfaces in a channel or duct to prevent a fully developed flow has been considered in many industrial applications. An extensive previous numerical study of the forced convection of air with interrupted fin surfaces or offset plates has been carried out for the compact heat exchanger such as Joshi and Webb (1987), Mizuno *et al.* (1994), Patanker and Prakash (1981), Sparrow and Liu (1979), Sparrow *et al.* (1977), and Suzuki *et al.* (1982; 1985). Peterson and Ortega (1990) presented a concise review of current work on the offset configuration in the thermal control of electronic equipment and devices. Through the literature review, most of presented work treated has been the convection heat transfer on the offset configuration considering isothermal or constant heat flux conditions, while the present knowledge of the long offset fins in the flow direction (offset plates' configuration), especially when it is neither subjected to constant heat flux nor having isothermal condition, i.e. heated by radiation heat flux, is not satisfactory, particularly for application to air heater solar collectors. Thus, to describe precisely the complex temporal and spatial structures of the effective heat transfer process, the physical system considered here for the numerical simulation analysis is conducted to investigate the laminar flow forced-convection heat transfer characteristics of air flow in a two parallel plates channel with offset absorber plates and heated by a radiation heat flux. Also in this study, the significance of design parameters on the convection heat transfer coefficient is investigated. These parameters are the optimum spacing of offset absorber plates relative to the nearest channel wall and the relation between an offset plate length and the channel hydraulic diameter for specified channel length. To obtain the convective heat transfer coefficient in this study, the velocity and temperature fields are obtained numerically by solving the two-dimensional, laminar-flow conservation equations. The flow field boundary temperatures are obtained by applying the energy balance to the boundary elements.

2. Physical model and analysis

The physical model considered in this study is shown in Figure 1. It consists of a two parallel plates channel formed by the back plate and the lower glass plate (g2). The back plate is an aluminum sheet coated with black paint on the upper side and thermally insulated from the back side, while, N numbers of aluminum plates are coated black on both sides forming the offset configuration. The upper glass plate (g1) is forming a convection shield between g2 and the ambient air.

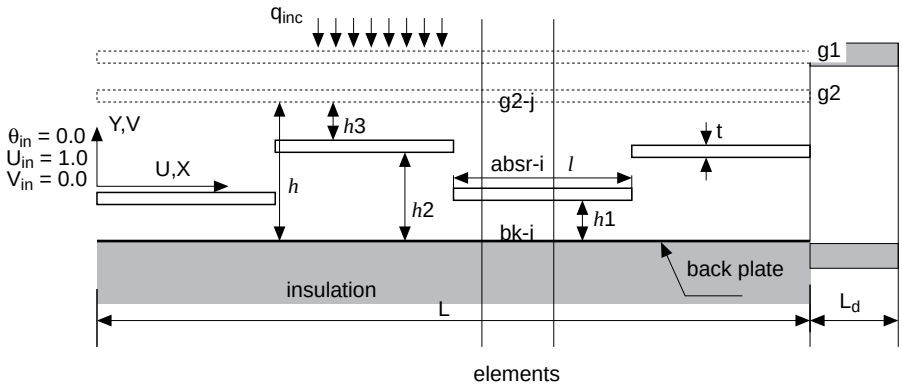

Figure 1.
Schematic of the two-dimensional physical system

2. 1 Flow field model

For the physical model shown in Figure 1, the flow is considered laminar, incompressible and the fluid (air) was assumed Newtonian with constant properties. The pressure work and viscous dissipation terms are negligible in the energy equation. The dimensionless equations that govern the steady-state of the conservation of mass, momentum and energy in the fluid portion in *X-Y* domain, obtained employing the Boussinesq approximation, and considering the natural convection are as follows:

$$\frac{\partial U}{\partial X}+\frac{\partial V}{\partial Y}=0 \tag{1}$$

$$U\frac{\partial U}{\partial X}+V\frac{\partial U}{\partial Y}=-\frac{\partial P}{\partial X}+\frac{1}{Re}\left(\frac{\partial^2 U}{\partial X^2}+\frac{\partial^2 U}{\partial Y^2}\right) \tag{2}$$

$$U\frac{\partial V}{\partial X}+V\frac{\partial V}{\partial Y}=-\frac{\partial P}{\partial Y}+\frac{Gr^*}{Re^2}\theta+\frac{1}{Re}\left(\frac{\partial^2 V}{\partial X^2}+\frac{\partial^2 V}{\partial Y^2}\right) \tag{3}$$

$$U\frac{\partial \theta}{\partial X}+V\frac{\partial \theta}{\partial Y}=\frac{1}{RePr}\left(\frac{\partial^2 \theta}{\partial X^2}+\frac{\partial^2 \theta}{\partial Y^2}\right) \tag{4}$$

The dimensionless variables employed in the above equations by taking the inlet velocity and the hydraulic diameter as the characteristic velocity and length are defined as follows:

$$X=\frac{x}{D_h},\quad Y=\frac{y}{D_h},\quad U=\frac{u}{u_{in}},\quad V=\frac{v}{u_{in}},\quad P=\frac{p}{\rho^{*}u_{in}^{2}},\quad Pr=\frac{\nu}{\alpha^{*}}\quad Re=\frac{u_{in}D_h}{\nu},$$

$$\theta=\frac{T-T_{in}}{\left(q_{rad,asbr}\frac{D_h}{k}\right)},\ \text{and}\quad Gr^{*}=\frac{g\beta q_{arad,absr}D_h^{4}}{k\nu^{2}} \tag{5}$$

All the flow field boundary, upper and lower surfaces of the offset plates, the upper surface of the back plate, and the lower surface of the lower glass cover, are assumed to be smooth, impermeable and non slip ($U = V = 0$) conditions. The inlet conditions of air (see Figure 1) are; $U_{in} = 1.0$, $V_{in} = 0$, and $\theta_{in} = 0$ respectively. The outflow boundary conditions at the channel outlet are taken to be $\frac{\partial U}{\partial X}(X,Y) = \frac{\partial V}{\partial Y}(X,Y) = 0$ and $\frac{\partial \theta}{\partial X}(X,Y) = 0$. The back side of the back plate is thermally insulated. The temperatures of the boundary surfaces imposed around the computational domain were obtained by applying the energy balance on each of the lower glass cover element (j) (g2-j), the offset plates element (i) (absr-i), and the back plate element (j) (bk-j) respectively as follows:

for (g2-j) $$q_{rad,g2}+q_{cond,g2}=q_{conv,g1,g2}+q_{conv,g2,air} \tag{6}$$

where $q_{rad,g2}$ is the net radiation heat flux absorbed in (g2-j) element (total absorbed radiation minus the emitted radiation) and its determination technique is given in the next section. $q_{cond,g2}$ is the net axial conduction heat flux onto (g2-j) element. $q_{conv,g1,g2}$ is the net natural convection heat flux between the two glass covers' elements. $q_{conv,g2,air}$ is the net convective heat flux loss/or gain from the lower glass cover element j to/or from the adjacent air stream element. It is calculated from the temperature difference between the near wall flow field temperature and the temperature of (g2-j) element.

for (absr-i) $$q_{rad,absr}+q_{cond,absr}=q_{conv,absr\text{-}u,air}+q_{conv,absr\text{-}l,air} \tag{7}$$

where $q_{rad,absr}$ is the net radiation heat flux absorbed in (absr-i) element (total absorbed radiation minus the emitted radiation) and its determination technique is given in the next section. $q_{cond,absr}$ is the net axial conduction heat flux onto (absr-i) element. $q_{conv,absr\text{-}u,air}$ and $q_{conv,absr\text{-}l,air}$ are the net convective heat flux transferred from the upper and lower surfaces of the offset plates element i to the adjacent air stream element. They are calculated from the temperature difference between the near wall flow field temperature and the temperature of (absr-i) element.

for (bk-j) $$q_{rad,bk}+q_{cond,bk}=q_{conv,bk,air} \tag{8}$$

where $q_{rad,bk}$ is the net radiation heat flux absorbed in (bk-j) element (total absorbed radiation minus the emitted radiation) and its determination technique is given in the next section. $q_{cond,bk}$ is the net axial conduction heat flux onto (bk-j) element. $q_{conv,bk,air}$ is the net convective heat flux loss/or gain

from the back plate element j to/or from the adjacent air stream element. It is calculated from the temperature difference between the near wall flow field temperature and the temperature of (bk-j) element.

2. 2 Net radiation heat transfer

The net absorbed radiation heat fluxes in the boundary surfaces' elements were obtained by using the ray tracing technique considering multiple reflection between those surfaces. The radiative heat transfer is divided into two bands, a shortwave band and longwave band (thermal radiation), and each band is treated separately using corresponding radiative properties.

2. 2. 1 Long-wave radiation (thermal radiation). The long-wave radiation heat fluxes absorbed in the lower glass cover, offset plates, and back plate elements are analyzed, knowing that glass cover plates are opaque to thermal radiation (long wave band). Also, both of the offset plates and the back plate are opaque to all radiation bands. All boundary surfaces are considered to be diffuse surfaces. The system shown in Figure 2 is confined to the lower surface of the absorber plate and the back plate. The method followed for analysis is by tracing a radiation beam leaving an element i of the lower surface of the absorber plate directed to element j of the back plate. The detailed multiple absorption and reflection between the offset absorber plate element i and the back plate element j is shown in Figure 2. The net thermal radiation heat flux absorbed in (bk-j) and (absr-i) elements from the thermal radiation emitted from all elements of the offset plates can thus be estimated as a function of the radiative properties of the enclosure, the configuration factors between the enclosure elements and their temperatures.

For back plate element j (bk-j). The radiation fraction absorbed in (bk-j) (see Figure 2) from the emitted thermal radiation from the offset plates lower surfaces (total elements), $q_{absr\text{-}l,bk\text{-}j,}$ can thus be estimated by using the series analysis as follows:

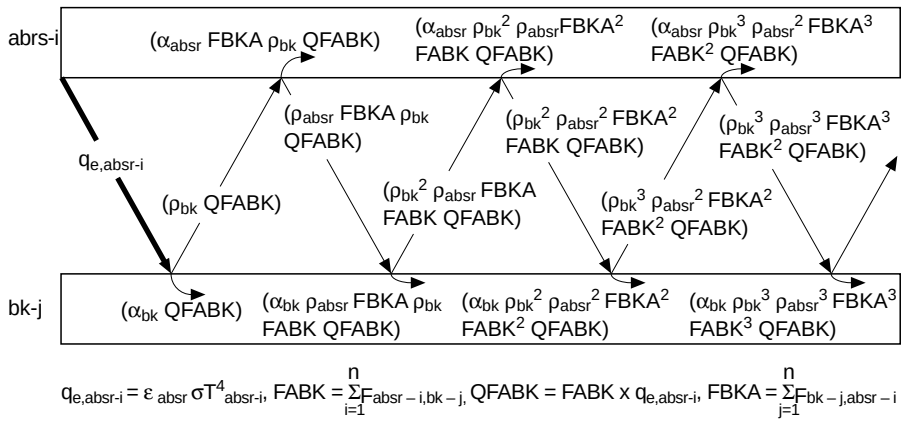

Figure 2.
Tracing of a long-wave radiation beam emitted from the lower surface of the offset plate element i towards the back plate

$$q_{absr\text{-}l,bk\text{-}j}=\alpha_{bk}\,QFABK+\alpha_{bk}\,\rho_{absr}\,FBKA\,\rho_{bk}\,FABK\,QFABK+\alpha_{bk}\,\rho_{absr}^{2}\,FBKA^{2}\,\rho_{bk}^{2}\,FABK^{2}\,QFABK+\alpha_{bk}\,\rho_{absr}^{3}\,FBKA^{3}\,\rho_{bk}^{3}\,FABK^{3}\,QFABK+\ldots \quad (9)$$

$$q_{absr\text{-}l,bk\text{-}j}=\alpha_{bk}\,QFABK\,(1+\rho_{absr}\,FBKA\,\rho_{bk}\,FABK+\rho_{absr}^{2}\,FBKA^{2}\,\rho_{bk}^{2}\,FABK^{2}+\rho_{absr}^{3}\,FBKA^{3}\,\rho_{bk}^{3}\,FABK^{3}+\ldots \quad (10)$$

using the series analysis equation (10) can be reduced into the following form:

$$q_{absr\text{-}l,bk\text{-}j}=\frac{\alpha_{bk}\,QFABK}{1-\rho_{absr}\,FBKA\,\rho_{bk}\,FABK} \quad (11)$$

The abbreviated quantities FABK, QFABK and FBKA in equation (11) are replaced by their values indicated in Figure 2, thus the final form of $q_{absr\text{-}l,bk\text{-}j}$ is given as follows:

$$q_{absr\text{-}l,bk\text{-}j}=\frac{\alpha_{bk}\,\varepsilon_{absr}\,\sigma\sum_{i=1}^{n}F_{absr\text{-}i,bk\text{-}j}\,T^{4}_{absr\text{-}i}}{1-\rho_{absr}\sum_{j=1}^{n}F_{bk\text{-}j,absr\text{-}i}\,\rho_{bk}\sum_{i=1}^{n}F_{absr\text{-}i,bk\text{-}j}} \quad (12)$$

For offset plates element i (absr-i). A similar procedure to that mentioned above can thus be used to estimate the absorbed thermal radiation fraction in the absorber plate element i from the lower surface of the total offset plates elements, $q_{absr\text{-}l,absr\text{-}i,}$ and is given as follows (see Figure 2):

$$q_{absr\text{-}l,absr\text{-}i}=\frac{\alpha_{absr}\,\varepsilon_{absr}\,\sigma\rho_{bk}\sum_{j=1}^{n}F_{bk\text{-}j,absr\text{-}i}\sum_{i=1}^{n}F_{absr\text{-}i,bk\text{-}j}\,T^{4}_{absr\text{-}i}}{1-\rho_{absr}\sum_{j=1}^{n}F_{bk\text{-}j,absr\text{-}i}\,\rho_{bk}\sum_{i=1}^{n}F_{absr\text{-}i,bk\text{-}j}} \quad (13a)$$

Following the same analysis and the terminology given above, the fraction of the thermal radiation absorbed in each element of the boundary surfaces from the emitted thermal radiation flux from all elements (including itself) $q_{bk,absr\text{-}i,}$ $q_{bk,bk\text{-}j,}$ $q_{absr\text{-}u,g2\text{-}j,}$ $q_{absr\text{-}u,absr\text{-}i}$, $q_{g2\text{-}l,absr\text{-}i,}$ $q_{g2\text{-}l,\,g2\text{-}j,}$ $q_{g2\text{-}u,g2\text{-}j,}$ and $q_{g1\text{-}l,g2\text{-}j,}$ can thus be obtained and are given as follows:

$$q_{bk,absr\text{-}i}=\frac{\alpha_{absr}\,\varepsilon_{bk}\,\sigma\sum_{j=1}^{n}F_{bk\text{-}j,absr\text{-}i}\,T^{4}_{bk\text{-}j}}{1-\rho_{absr}\sum_{j=1}^{n}F_{bk\text{-}j,absr\text{-}i}\,\rho_{bk}\sum_{i=1}^{n}F_{absr\text{-}i,bk\text{-}j}} \quad (13b)$$

$$q_{bk,bk\text{-}j}=\frac{\alpha_{bk}\,\varepsilon_{bk}\,\sigma\rho_{absr}\sum_{i=1}^{n}F_{absr\text{-}i,bk\text{-}j}\sum_{j=1}^{n}F_{bk\text{-}j,absr\text{-}i}T^{4}_{bk\text{-}j}}{1-\rho_{absr}\sum_{j=1}^{n}F_{bk\text{-}j,absr\text{-}i}\,\rho_{bk}\sum_{i=1}^{n}F_{absr\text{-}i,bk\text{-}j}} \tag{13c}$$

$$q_{absr\text{-}u,g2\text{-}j}=\frac{\alpha_{g2}\,\varepsilon_{absr}\,\sigma\sum_{i=1}^{n}F_{absr\text{-}i,g2\text{-}j}\,T^{4}_{absr\text{-}i}}{1-\rho_{absr}\sum_{j=1}^{n}F_{g2\text{-}j,absr\text{-}i}\,\rho_{g2}\sum_{i=1}^{n}F_{absr\text{-}i,g2\text{-}j}} \tag{13d}$$

$$q_{absr\text{-}u,absr\text{-}i}=\frac{\alpha_{absr}\,\varepsilon_{absr}\,\sigma\rho_{g2}\sum_{j=1}^{n}F_{g2\text{-}j,absr\text{-}i}\sum_{i=1}^{n}F_{absr\text{-}i,g2\text{-}j}\,T^{4}_{absr\text{-}i}}{1-\rho_{absr}\sum_{j=1}^{n}F_{g2\text{-}j,absr\text{-}i}\,\rho_{g2}\sum_{i=1}^{n}F_{absr\text{-}i,g2\text{-}j}} \tag{13e}$$

$$q_{g2\text{-}l,absr\text{-}i}=\frac{\alpha_{absr}\,\varepsilon_{g2}\,\sigma\sum_{j=1}^{n}F_{g2\text{-}j,absr\text{-}i}\,T^{4}_{g2\text{-}j}}{1-\rho_{absr}\sum_{j=1}^{n}F_{g2\text{-}j,absr\text{-}i}\,\rho_{g2}\sum_{i=1}^{n}F_{absr\text{-}i,g2\text{-}j}} \tag{13f}$$

$$q_{g2\text{-}l,g2\text{-}j}=\frac{\alpha_{g2}\,\varepsilon_{g2}\,\sigma\rho_{absr}\sum_{i=1}^{n}F_{absr\text{-}i,g2\text{-}j}\sum_{j=1}^{n}F_{g2\text{-}j,absr\text{-}i}T^{4}_{g2\text{-}j}}{1-\rho_{absr}\sum_{j=1}^{n}F_{g2\text{-}j,absr\text{-}i}\,\rho_{g2}\sum_{i=1}^{n}F_{absr\text{-}i,g2\text{-}j}} \tag{13g}$$

$$q_{g2\text{-}u,g2\text{-}j}=\frac{\alpha_{g2}\,\varepsilon_{g2}\,\sigma\rho_{g1}\sum_{i=1}^{n}F_{g1\text{-}i,g2\text{-}j}\sum_{j=1}^{n}F_{g2\text{-}j,g1\text{-}i}\,T^{4}_{g2\text{-}j}}{1-\rho_{g2}\sum_{j=1}^{n}F_{g2\text{-}j,g1\text{-}i}\,\rho_{g1}\sum_{i=1}^{n}F_{g1\text{-}i,g2\text{-}j}} \tag{13h}$$

$$q_{g1\text{-}l,g2\text{-}j}=\frac{\alpha_{g2}\,\varepsilon_{g1}\,\sigma\sum_{i=1}^{n}F_{g1\text{-}i,g2\text{-}j}\,T^{4}_{g1\text{-}i}}{1-\rho_{g1}\sum_{j=1}^{n}F_{g2\text{-}j,g1\text{-}i}\,\rho_{g2}\sum_{i=1}^{n}F_{g1\text{-}i,g2\text{-}j}} \tag{13i}$$

2. 2. 2 Short-wave radiation. Following the procedure mentioned above for longwave radiation band, the absorbed portions in (g2-j) and (absr-i) elements in the shortwave radiation band can be estimated. Those portions are from the direct incident radiation heat flux and the fraction absorbed from that reflected from two adjacent elements by using the ray tracing technique. The absorbed shortwave radiation portions are obtained with the following assumptions, the glass cover plates are adequately characterized by their shortwave and long-wave band radiation properties, the offset plates and the back plate are opaque to all radiation bands, and, no radiation passes through the clearance distance of the offset plates.

As shown in Figure 1, the upper glass cover plates (g1) receive incident radiation from the radiation heat flux source. The absorbed shortwave radiation portions in (g2-j) and (absr-i) elements can thus be estimated as follows;

$$q_{abs,g2\text{-}j)_{sw}} = q_{inc}\left\{\tau_{g1}\,\alpha_{g2}\left[1+\frac{\rho_{absr}\,\tau_{g2}}{1-\rho_{absr}\,\rho_{g2}}+\frac{\rho_{absr}\tau^{2}_{g2}\,\rho_{g1}+\rho_{g1}\,\rho_{g2}}{1-\rho_{g1}\,\rho_{g2}}\right]\right\}_{sw} \tag{14}$$

$$q_{abs,absr\text{-}i)_{sw}} = q_{inc}\left\{\tau_{g1}\tau_{g2}\,\alpha_{absr}\left[\frac{1}{1-\rho_{absr}\,\rho_{g2}}+\frac{\rho_{absr}\,\rho_{g1}\,\rho_{g2}+\rho_{g1}\,\rho_{g2}}{1-\rho_{g1}\,\rho_{g2}}\right]\right\}_{sw} \tag{15}$$

2. 2. 3 Total absorbed radiation. The total absorbed radiation fluxes (W/m^2) in each element were estimated by summing both the absorbed fraction in the shortwave and the longwave radiation bands and are given by:

$$\underline{\text{for (g2-j)}}\quad q_{abs,g2\text{-}j} = q_{abs,g2)_{sw}} + q_{absr\text{-}u,g2\text{-}j} + q_{g2\text{-}l,g2\text{-}j} + q_{g2\text{-}u,g2\text{-}j} + q_{g1\text{-}l,g2\text{-}j} \tag{16}$$

$$\underline{\text{for (absr-i)}}\quad q_{abs,absr\text{-}i} = q_{abs,absr\text{-}i)_{sw}} + q_{absr\text{-}l,absr\text{-}i} + q_{bk,absr\text{-}i} + q_{absr\text{-}u,absr\text{-}i} + q_{g2\text{-}l,absr\text{-}i} \tag{17}$$

$$\underline{\text{for (bk-j)}}\quad q_{abs,bk\text{-}j} = q_{absr\text{-}l,bk\text{-}j} + q_{bk,bk\text{-}j} \tag{18}$$

2. 2. 4 Total emitted radiation. The total emitted thermal radiation flux from the boundaries elements can be estimated as follows:

$$\underline{\text{for (g2-j)}}\quad q_{emit,g2\text{-}j} = 2\sigma\,\varepsilon_{g2,lw}\,T^{4}_{g2\text{-}j} \tag{19}$$

$$\underline{\text{for (absr-i)}}\quad q_{emit,absr\text{-}i} = 2\,\sigma\,\varepsilon_{absr\text{-}i,lw}\,T^{4}_{absr\text{-}i} \tag{20}$$

$$\underline{\text{for (bk-j)}}\quad q_{emit,bk\text{-}j} = \sigma\,\varepsilon_{bk\text{-}j,lw}\,T^{4}_{bk\text{-}j} \tag{21}$$

The net absorbed radiation flux $q_{rad,g2-j,}$ $q_{rad,absr-i}$ and $q_{rad,bk-j}$ in (g2-j), (absr-i), and (bk-j) elements can thus be calculated as the total absorbed flux minus the total emitted flux quantities.

The configuration factors between surfaces are estimated using the general relation of two infinitely long, directly opposed parallel plates of the same finite width that were presented in Siegel and Howell (1991). Knowing the configuration factors between such surfaces, for example (absr-i, i = 1) and (bk-j, j = 1, 2, 3, …, n), and from geometrical similarity, one can compute the configuration factor between any surfaces by applying the reciprocity relations.

2. 3 Convection heat transfer coefficient presentation parameters

During execution of the solutions, the bulk temperature $T_{b,x}$ at any axial location X was determined by integration of the θ and U distribution as follows:

$$\frac{T_{b,x}-T_{in}}{\left(q_{rad,absr}\frac{D_h}{k}\right)}=\theta_b=\frac{\int\theta U dY}{\int U dY} \qquad 0 \le Y \le h/D_h \tag{22}$$

Existing local Nusselt number (Nu_x) relation involving both offset plates sides convection heat transfer is defined as follows:

$$Nu_x=\frac{D_h}{k_{air}}\left(\frac{q_{conv,absr-u,air}+q_{conv,absr-l,air}}{T_{absr,x}-T_{b,x}}\right) \tag{23}$$

where $q_{conv,absr-u,air}$ and $q_{conv,absr-l,air}$ are the convective heat fluxes from the upper and lower surfaces of offset absorber plates element i (absr-i).

In discussions of the computational results the average Nusselt number $\overline{Nu}$ is used and is defined as follows:

$$\overline{Nu}=\frac{1}{N}\int_{Pl=1}^{N}\overline{Nu_{pl}} \quad \text{where} \quad \overline{Nu_{pl}}=\frac{1}{\ell}\int_{x=0}^{\ell}Nu_x\,dx \tag{24}$$

2. 4 Numerical method of solution

The governing equations (1) to (4) of the continuity, momentum and energy for the flow field were solved numerically. Computations were performed using routine finite-difference methods. The flow field-pressure velocity coupling is treated by the SIMPLE algorithm of Patankar (1980), more details of the numerical procedure are presented in Katsuki and Nakayama (1990). The control volume has **h** height and total length $L + L_d$, where L_d is the downstream length of computational domain required for numerical stability as

shown in Figure 1. The chosen ratio of $L_d/\mathbf{l}$ was large enough (namely, $L_d/\mathbf{l}$ = 0.4, for this entire study) to ensure the stability condition. Therefore, the flow field at the exit from the trailing edge of the last offset plate is not sensitive to further increase to this value.

The temperatures of the boundary elements were obtained by solving the energy balance equations (6) to (8) for n-module model, generating $(3 \times n)$ finite central difference nonlinear equations in $(3 \times n)$ unknowns. These unknown $(3 \times n)$ are the temperatures of the back plate, offset plates, and lower glass cover elements respectively. For solving this set of nonlinear heat balance equations, the multidimensional secant method – Broyden's method – as presented in Press *et al.* (1992) was used.

The radiative properties used in calculations of the radiation part of the model were measured values, their measuring technique was described in Ali *et al.* (1998). The average measured values of the absorptance and reflectance, for offset plates and the back plate samples, those coated black paint with coating thickness of about 60 μm, in the wavelength ranged from 0.3 to 17 μm were about 0.94 and 0.06 respectively, while the glass covers plates (g1) and (g2) are ordinary float colorless sheets of 3mm thickness, and having an average normal transmittance, reflectance and absorptance in the spectrum range of 0.3 to 3.0 μm are 0.855, 0.05 and 0.095 respectively. The absorptance and reflectance of (g1) and (g2) in longwave band (more than 3.0 μm) are 0.85 and 0.15 respectively.

The incident radiation flux was set equal to 1,000.0 W/m^2, the Prandtl number was set equal to 0.72 and the Re number was varied from 500 to 2,550. In this range of Re, the real flow is expected to be mostly laminar, although a small value of $t/\mathbf{l}$, it is possible that transition to turbulence may occur somewhat before Re = 2,550. Also, the real flow may display instabilities and vortex-shedding from the trailing edges of the plates, especially the last one. These phenomena are beyond the scope of the present numerical simulation study. The base case of the dimensions for Figure 1 used in the present computations are as follows, N = 4, L = 864mm, $\mathbf{h}$ = 26mm, t = 1mm, $\mathbf{l}$ = 216mm and D_h = 48.6mm respectively.

For the grid system, a refinement study was performed to select uniform grid numbers, particularly in X direction. Thus, this selection will not only affect on the accuracy, stability, scalability of the computer program and time required for the calculation of the whole domain (the calculation is carried on PC) but also on the numerical stability of the radiation part of the model. It was found that the grid points of total numbers 270×52 that allocated uniformly, to ease solving the radiation model for the temperature boundary conditions, gives reasonable output results in comparison with experimental results' values.

The flow field computation was started with artificial temperatures of the surfaces' boundary elements. Then, this first stage flow field computed results of U, V, and θ are used in solving the energy balance equations (6) to (8) to get the temperatures of the surfaces boundary elements. These new

temperatures of the surfaces' boundary elements are used to solve the flow field again in the second stage. These computation procedures are repeated until the change in the temperatures of the surfaces' boundary elements became within the allowable error. The solution procedure is iterative for all variables and the computation was terminated when the sum of the absolute residuals normalized by the inflow fluxes were below 10^{-7} for all the variables. This residual can be obtained at 8,000 iterations for Re = 2,550 and at 10,000 iterations for Re = 650 or less, for the total number of grid points was 270×52.

3. Results and discussion

3.1 Validity of the numerical simulation results

3.1.1 Temperature distribution. Figure 3 shows the comparison between the experimentally measured temperatures' values presented in Ali *et al.,* (1998) and their corresponding values obtained from the numerical model for the temperature's distribution of the offset plates, back plate, lower glass plate and air bulk respectively. It is clear from the figure that the predicted temperature values of the offset plates, back plate and air bulk temperatures are in good agreement with the measured data, while for the lower glass cover there is a

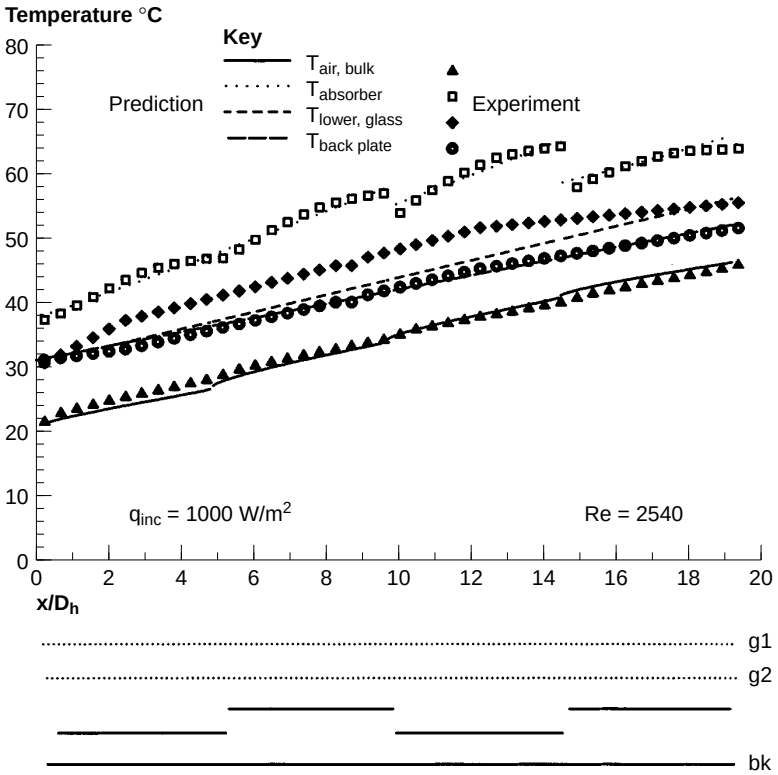

Figure 3.
Verification of temperatures numerically calculated with measured values of Ali *et al.* (1998)

deviation between the predicted and measured temperatures at a location close to the leading edge of the first offset plate up a location near the x/D_h =17. This can be attributed to using an approximate relation to calculate the free convection heat transfer between the two glass plates, while the main aim of this study is focused on the offset plates, where both experimental and numerical temperatures' results agree well. However, this good agreement gives confidence on the radiation part of the model to describe the temperatures of the surfaces' boundary elements with reasonable accuracy.

3.1.2 Local Nusselt number. Figure 4 shows the comparison between the experimentally calculated as presented in Ali *et al.,* (1998) and numerically predicted values of the local Nusselt number in case of N = 4, incident radiation flux equal 1,000 W/m^2 and Re numbers of 650 and 2,550. As seen from the figure, there are noticeable differences among the two Re numbers around the

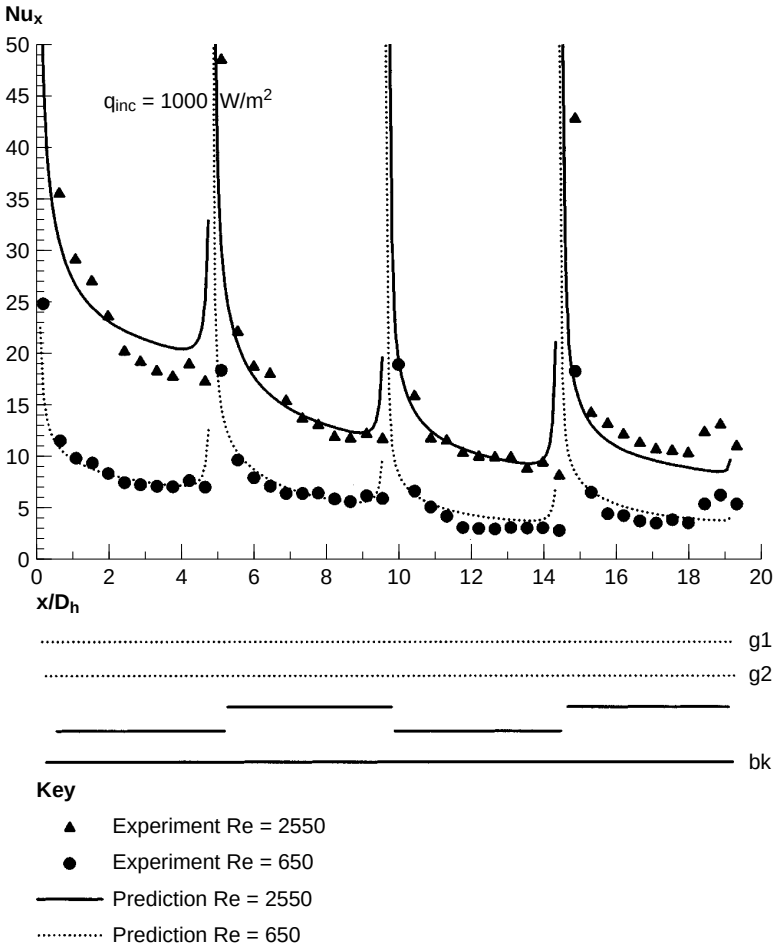

Figure 4.
Comparison of numerically predicted local Nusselt number with experimentally calculated values of Ali *et al.* (1998) for Re = 650 and 2,550 respectively

trailing edge of each plate. This difference can be attributed to the vortex-shedding flow from the trailing edge of each offset plate in the experimental results, while this phenomenon is out of the scope of the present numerical simulation. Also, it can be seen from the figure, for low Reynolds number (Re = 650) there is a good agreement between the experimentally calculated and numerically predicted values of the local Nusselt number (Nu_x) up to a short distance before the trailing edge of each offset plate, while for high Reynolds number (Re = 2,550) the experiment shows a slightly higher value of the local Nusselt number (Nu_x) in comparison with the numerical results, particularly for the 1st and 4th offset plates. This may be due to choice of uniform grid in this study, and this effect is clear for Re = 2,550, particularly, at the inlet and outlet from the channel, while it does not appear for Re = 650. This is due to the flow around each offset plate for Re = 2,550 being a developing one, while this condition is not for Re = 650. However, the reasonable agreement between the experimental and numerical computation validates the numerical scheme to perform a parametric study on effects of geometric and design parameters on the convective heat transfer coefficient.

3.2 Effect of Re number on the flow and temperature fields

Before reporting and discussing the effect of the design parameters on the convection heat transfer coefficient, discussing the effect of Re number on the flow and temperature fields will be made. However, knowledge of the effect of Re number on the flow and temperature fields is helpful when discussing the effect of other design parameters. This was done by presenting the flow pattern (velocity vector field) and temperature fields, those obtained from the numerical results for Re = 500 and 2,550 as shown in Figure 5. As seen from the figure, at low Re number (Re = 500, Figure 5(a)) both the hydrodynamic (velocity vector field) and the thermal entrance lengths (air temperature distributions-isothermal lines) are close to the leading edge of each offset plate. Thus, the flow field around each offset plate, after a short distance from the leading edge, is almost fully developed thermally and hydrodynamically. Also, it can be seen from the figure, the flow wake as well as the thermal wake is smooth and occupying a small zone behind the trailing edge of each offset plate. Thus, the flow field appears to be fully recovered at a short distance from the trailing edge of each offset plate. For higher Re number (Re = 2,550, Figure 5(b)), both the hydrodynamic and thermal entrance lengths are up to or larger than the trailing edge of each offset plate. Thus, the flow field around each offset plate is a developing one. Also, the development of the thermal and flow wakes (see the velocity vector profile and isothermal lines of Figure 5(b)) formed after the trailing edge of each offset plate is obvious and those wakes affect the flow over each downstream offset plate. However, wake flow fills the space between the trailing edge of one offset plate and the leading edge of the next one. Thus, the velocity vector profile indicates the flow field is still not fully recovered between

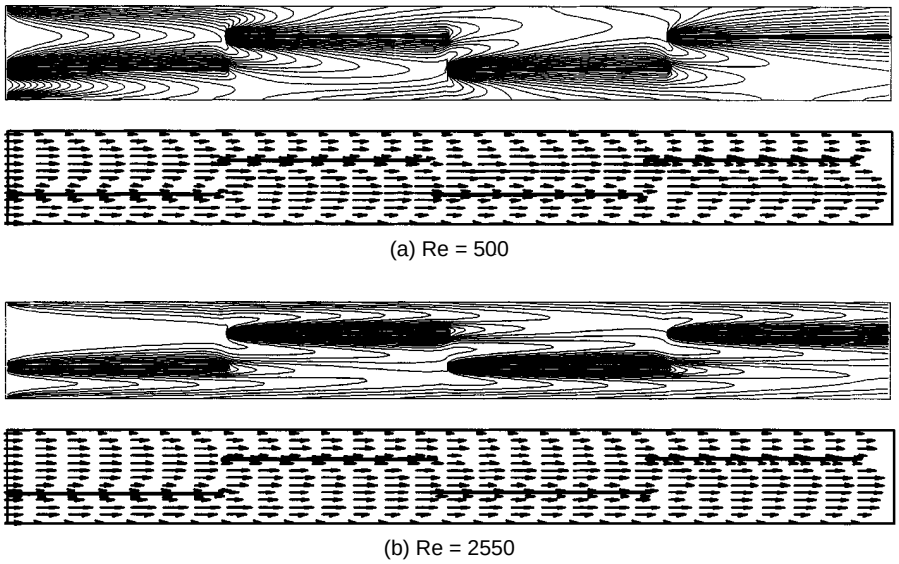

Figure 5.
Flow patterns (velocity vector field) and temperature contour maps of air

two offset plates, and that causes the mixing level to be much higher than that in case of low Re number.

3.3 Optimum spacing of offset plates relative to channel walls

While the offset plates provide a high heat transfer coefficient compared with one continuous plate, one of the fundamental thermal design questions can be addressed; what is the optimal offset plate spacing relative to the nearest channel walls (the lower glass cover and back plate). An optimizing of offset plate spacing h1 and h3 of Figure 1 for two mass flow rates corresponding to the two Re numbers of 650 and 2,550 was accomplished using this numerical model. Figure 6 shows the average Nusselt number with the ratio (h1 + h3)/h (where h1 = h3) for the two values of Re number. As seen from the figure, the average Nusselt number values increase as the offset plate height decreases relative to the nearest channel walls. Thus, up to around one third of the gap h, h1 = h3 = h/3, the average Nusselt number values decreased again for both values of Re. This can be attributed to the velocity defect in the wake behind the trailing edge of each offset plate being restored faster as the gap (h-h1) or (h-h3) increasing up to around certain values refers to Figure 7. Then this process decreases again. Therefore, those results homogeneously in the air bulk temperature before the leading edge of the next downstream offset plate, that provides a condition for rebuilding a thinning velocity and temperature boundary layer on the next one. Also, it is shown in Figures 6 and 7 that, for Re = 650, the higher value of the average Nusselt number can be obtained at a ratio (h1 + h3)/h = 0.7, while for Re = 2,550 it can be obtained at a ratio (h1 + h3)/h = 0.65. This slight difference is explained, referring to Figure 7, to the

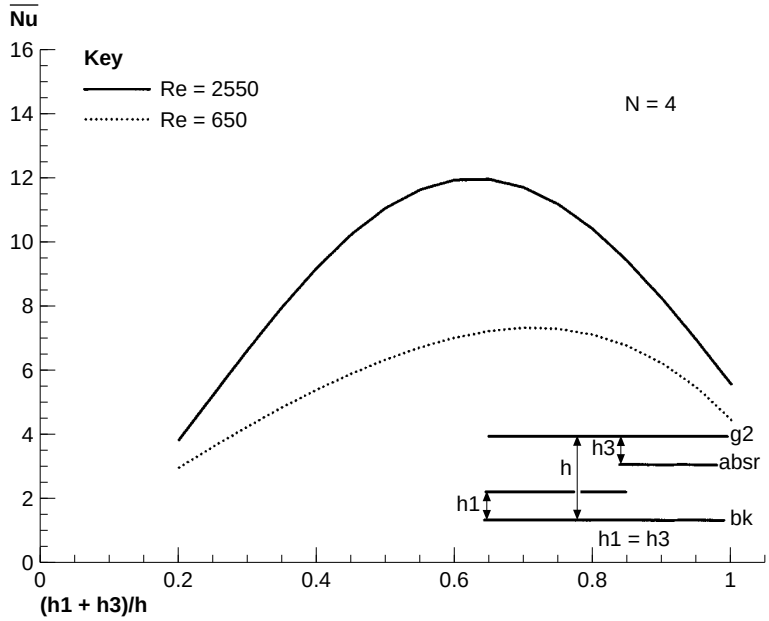

Figure 6.
Effect of offset plate spacing relative to channel walls on the average Nusselt number for two values of Re number

wakes after the trailing edge being dependent on the distance (h1/h) or (h3/h) as explained above and on the effect of the Re number on the flow field as explained in section (3.2). Both of those factors produce this slight change of the optimum space relative to the channel walls for the two Re numbers. This leads to the conclusion that the best position of each offset plate relative to the nearest wall of the parallel plates channel is to be near one third of the channel height, and the worst position is in the middle or close to its walls.

3. 4 Effect of the number of the offset plates on the convective heat transfer coefficient

The second thermal design aspect that can be investigated here is the number of the offset plates N that leads to a higher heat transfer coefficient in case of a constant channel length L, i.e. the offset plate length where $N = L/l$. In the other meaning, the relation between one offset plate length and the hydraulic diameter. This will be obtained by assuming that the N offset plates are positioned at h1 = h3 = h/3 of Figure 1, in accordance with the conclusions reached in the preceding section. Figure 8 shows the variation of $\overline{Nu}$ with (D_h/l) or N for the case, when the total length of the offset plates L (see Figure 1) is unchanged. As shown in the figure, $\overline{Nu}$ increases as D_h/l increases (or, N increases). Thus, for a certain hydraulic diameter, always a shorter length of offset plate is better for a higher convective heat transfer coefficient. However, the rate of the increase of $\overline{Nu}$ is rather small when $D_h/l > 0.562$ (or, $N > 10$) in case of Re = 2,550, while it is rather small when $D_h/l > 0.675$ (or, $N > 12$) in case

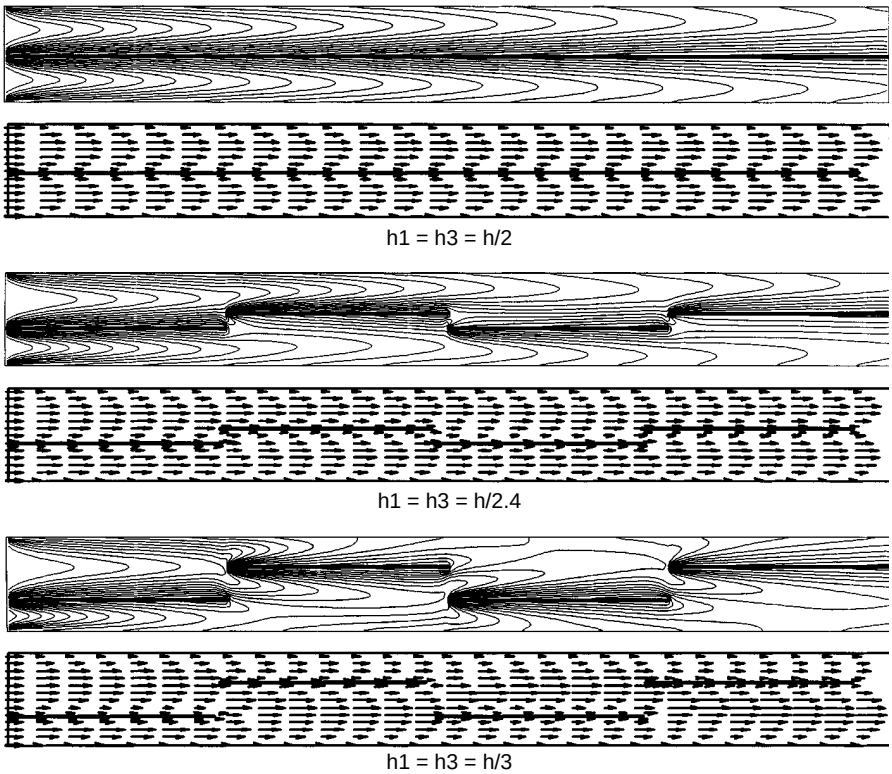

Figure (7a).
Flow patterns and temperature contour maps of air for different offset plate spacing relative to the nearest wall for Re = 650, (h1 + h3)/h = 1.0 and N = 4

of Re = 650. This can be explained as it can be seen from Figure 9, as follows, at Re = 650 both the hydrodynamic and the thermal entrance length being close to the leading edge of each offset plate. Thus, as the number of the offset plates increases there is an excessive interruption of the flow field that leads to an increase in the convection heat transfer coefficient. Thus, excessive interruption of the velocity and temperature boundary layers is not more efficient for $D_h/l \leq 0.675$ ($N \geq 12$), while for Re = 2,550 both of the hydrodynamic and the thermal entrance lengths are up to or larger than the trailing edge of each offset plate. Thus, excessive interruption of the velocity

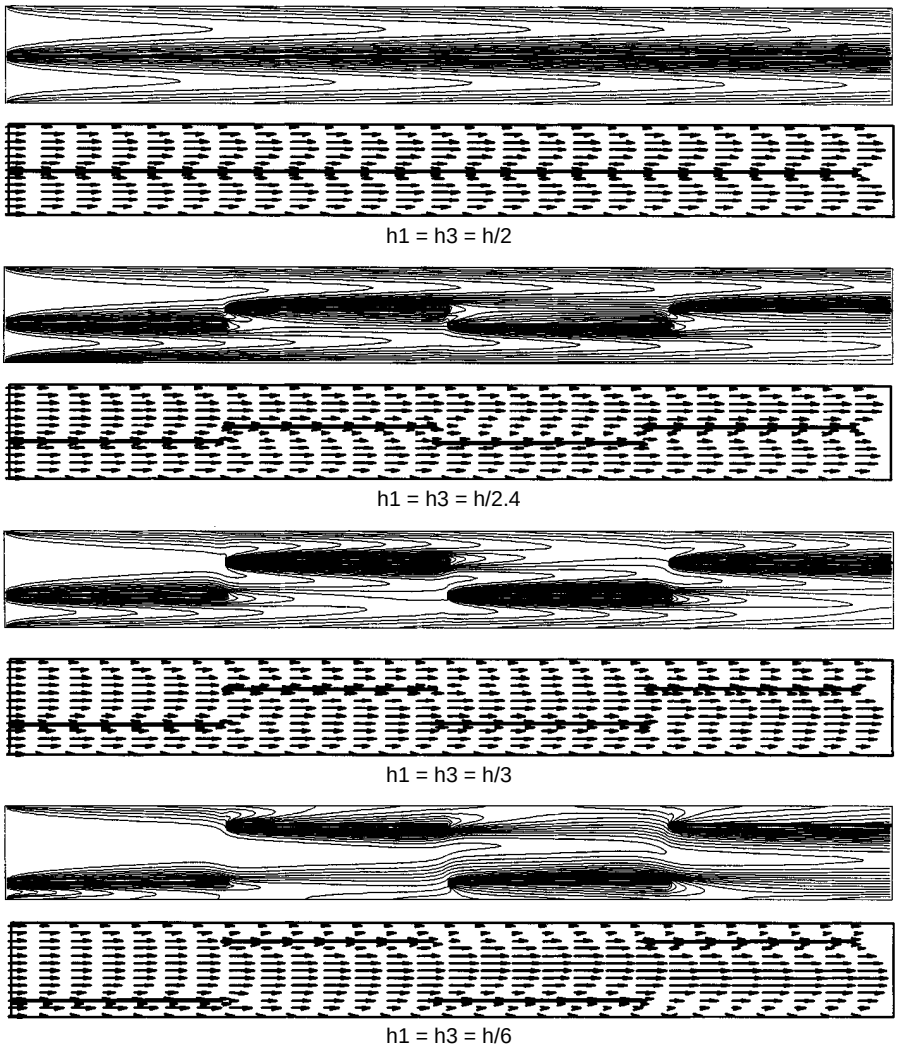

Figure (7b). Flow patterns and temperature contour maps of air for different offset plate spacing relative to the nearest wall for Re = 2550, (h1 + h3)/h = 1.0 and N = 4

and temperature boundary layers is not efficient for $D_h/l \leq 0.562$ ($N \geq 10$). Air heaters solar collectors normally work in Re numbers ranging from 500 to 2,500, to obtain a reasonable temperature difference through the collector. However, based on the results shown in Figure 8, the offset plate length would be around one and half times the hydraulic diameter of the two parallel plates flow channel. Using such an offset plate length less than this ratio (increasing the number of the offset plates) is not more efficient for convective heat transfer and of course will certainly be accompanied by an increase in manufacturing cost.

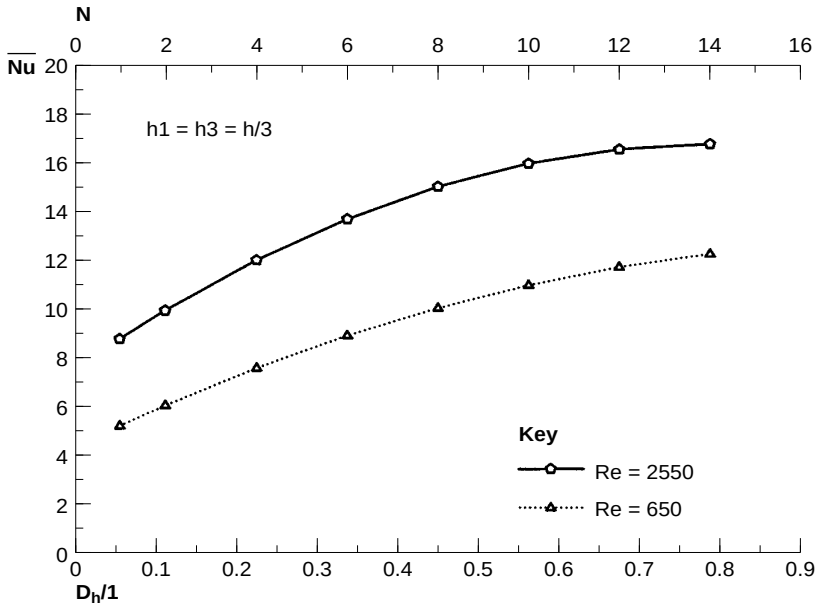

Figure 8.
Effect of offset plate length relative to hydraulic diameter (offset plate numbers) on the average Nusselt number for two values of Re number

3. 5 Correlations of the average Nusselt number

Using output data results of the numerical model of the effect of the ratio D_h/l on $\overline{Nu}$, a correlation of the average Nusselt number ($\overline{Nu}$) as a function of Re number, Pr number, and the ratio (D_h/l) for Re number ranging from 500 to 2,550 and h1 = h3 = h/3. The correlation is given as follows;

$$\overline{Nu} = 1.81\ Re^{0.352}\ Pr^{1/3}\ (D_h/\ell)^{1/2} \tag{25}$$

4. Conclusions

A forced laminar convection heat transfer on air flowing in two parallel plate channel with offset plates and heated by radiation heat flux was investigated by the numerical simulation study of a two-dimensional model. The numerical simulation results were verified by experimental results and show a qualitatively good agreement. The numerical simulation results show that the optimum offset plate spacing relative to the nearest wall of two parallel plates was found to be around the number of one third of the channel wall height in Re number ranging from 650 to 2,550 (Figure 9). Also, in this range of Re numbers, the optimum offset plate numbers can be calculated based on the offset plate length as being around one and half times the hydraulic diameter of the two parallel plates flow channel. Using the data obtained from this study, a correlation of the average Nusselt number can be given as follows; $\overline{Nu} = 1.81\ Re^{0.352}\ Pr^{1/3}\ (D_h/l)^{1/2}$.

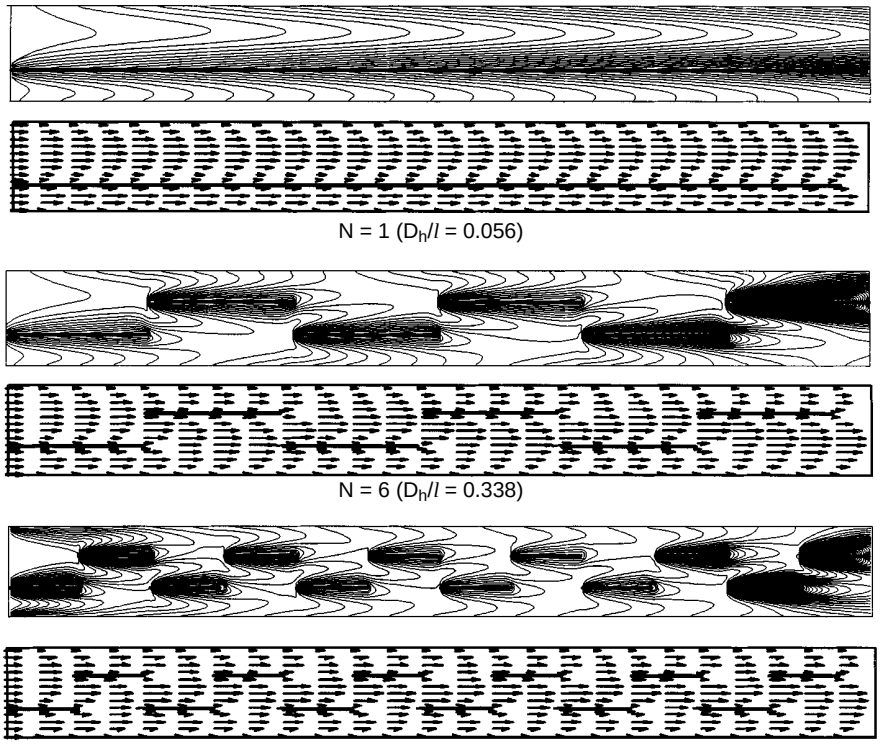

Figure 9.
Flow patterns and temperature contour maps of air for different offset plate number (a) for Re = 650; (b) for Re = 2,550)

References

Ali, A.H.H., Hanaoka, Y., Kishinami, K. and Suzuki, J. (1998), "Experimental study of laminar flow forced-convection heat transfer in air flowing through offset plates heated by radiation heat flux", *Int. J. comm. Heat Mass Transfer,* (in press).

Joshi, H.M. and Webb, R. (1987), "Heat transfer and friction in offset strip-fin heat exchanger", *Int. J. Heat Mass Transfer,* Vol. 30, pp. 69-84.

Katuski, M. and Nakayama, A. (1990), *Numerical Simulation of Heat and Fluid Flow-Fundamentals of Programming,* Morikita Publishing Co., Tokyo (in Japanese).

Mizuno, M., Hori, M. and Kudo, K. (1994), "Heat transfer and flow characteristics of offset fins in low-Reynolds-number region (effect of thermal conductivity)", *Trans. JSME* B 60-569, pp. 263-9.

Patankar, S.V. (1980), *Numerical Heat Transfer and Fluid Flow,* Hemisphere/McGraw-Hill, Washington.

Patankar, S.V. and Prakash, C. (1981), "An analysis of the effect of plate thickness on laminar flow and heat transfer in interrupted-plate passages", *Int. J. Heat Mass Transfer,* Vol. 24, pp. 1801-10.

Peterson, G.P. and Ortega, A. (1990), "Thermal control of electronic equipment and devices", *Adv. Heat Transfer,* Vol. 20, pp. 181-314.

Press, W.H., Teukolsky, S.A., Vetterling, W.T. and Flamery, B.P. (1992), *Numerical Recipes in Fortran – The Art of Scientific Computing,* 2nd ed., Cambridge University Press.

Siegel, R. and Howell, J.R. (1991), *Thermal Radiation Heat Transfer,* P. 300, 3rd ed., Hemisphere Publishing Co.

Sparrow, E.M. and Liu, C.H. (1979), "Heat-transfer, pressure-drop and performance relationship for in-line, staggered, and continuous plate heat exchangers", *Int. J. Heat Mass Transfer,* Vol. 22, pp. 1613-25.

Sparrow, E.M., Baliga, B.R. and Patankar, S.V. (1977), "Heat transfer and fluid flow analysis of interrupted-wall channels, with application to heat exchangers", *J. of Heat Transfer,* Vol. 99, pp. 4-11.

Suzuki, K., Hirai, E., Miyake, T. and Sato, T. (1985), "Numerical and experimental studies on a two-dimensional model of an offset-strip-fin type compact heat exchanger used at low Reynolds number", *Int. J. Heat Mass Transfer,* Vol. 28, pp. 823-36.

Suzuki, K., Hirai, E., Sato, T. and Kieda, S. (1982), "Numerical study of heat transfer system with staggered array of vertical flat plates used at low Reynolds number", *Proc. of the 7th Int. Heat Transfer Conf.* Vol. 3, pp. 483-8.